

## IUPAC Task Group on Atmospheric Chemical Kinetic Data Evaluation – Data Sheet P4

Datasheets can be downloaded for personal use only and must not be retransmitted or disseminated either electronically or in hardcopy without explicit written permission.

The citation for this datasheet is: Atkinson, R., Baulch, D. L., Cox, R. A., Crowley, J. N., Hampson, R. F., Hynes, R. G., Jenkin, M. E., Rossi, M. J., and Troe, J.: Atmos. Chem. Phys. 4, 1461, 2004; IUPAC Subcommittee for Gas Kinetic Data Evaluation, (<http://iupac.pole-ether.fr>).

This datasheet last evaluated: May 2013; last change in preferred values: May 2013.

### (CHO)<sub>2</sub> + hv → products

#### Primary photochemical transitions

Reaction		$\Delta H^{\circ}_{298}/\text{kJ}\cdot\text{mol}^{-1}$	$\lambda_{\text{threshold}}/\text{nm}$
(CHO) <sub>2</sub> + hv → H <sub>2</sub> + 2CO	(1)	-9.1	-
→ 2HCO	(2)	298.1	413
→ HCHO + CO	(3)	-7.2	-
→ H + HC(O) + CO	(4)	362.5	342
→ 2H + 2CO	(5)	426.9	291

#### Absorption cross-section data

Wavelength range/nm	Reference	Comments
230-462	Plum <i>et al.</i> , 1983	(a)
210-450	Orlando and Tyndall, 2001	(b)
210-480	Horowitz <i>et al.</i> , 2001	(c)
250-526	Volkamer, <i>et al.</i> , 2005	(d)

#### Quantum yield data ( $\phi = \phi_1 + \phi_2 + \phi_3 + \phi_4 + \phi_5$ )

Measurement	Wavelength range/nm	Reference	Comments
$\phi = 0.029 \pm 0.018$	325-470	Plum <i>et al.</i> , 1983	(e)
$\phi(\text{HCO}) = 0.8 \pm 0.4$	308	Langford and Moore, 1984	(f)
$\phi(\text{HCO}) = 0.42 \pm 0.22$	193	Zhu <i>et al.</i> , 1996	(g)
$= 0.54 \pm 0.24$	248		
$= 0.70 \pm 0.30$	308		
$= 1.5 \pm 0.6$	351		
$\phi^{\circ}(\text{HCO}) = 0.50 \pm 0.01$	290	Chen and Zhu, 2003	(h)
$= 0.84 \pm 0.07$	310		
$= 1.77 \pm 0.12$	330		
$= 1.34 \pm 0.06$	350		
$= 1.49 \pm 0.04$	370		
$= 2.01 \pm 0.08$	390		
$= 0.56 \pm 0.04$	410		

$\phi = 0.97 \pm 0.05$	275-380	Tadjic et al., 2006	(i)
$\phi = 0.12$ (133 mbar)	390-470		
$\phi = 0.042$ (931 mbar)	390-470		
$\phi^0(\text{HCO}) = 0.38 \pm 0.03$	290	Feierabend, et al, 2009	(j)
= $0.62 \pm 0.09$	311		
= $1.68 \pm 0.34$	330		
= $1.74 \pm 0.24$	350		
= $1.85 \pm 0.27$	370		
= $1.69 \pm 0.84$	390		
= $0.14 \pm 0.02$	416		
$\phi(\text{HCO}) = 1.19 \pm 0.06$	335	Salter et al., 2013a	(k)
= $1.08 \pm 0.04$	320		
= $0.71 \pm 0.08$	310		
$\phi(\text{H}) = 0.95 \pm 0.12$	193		
= $0.39 \pm 0.12$	308		
= $0.32 \pm 0.02$	308		
= $0.27 \pm 0.07$	316.7		
= $0.18 \pm 0.15$	339.7		
$\phi = 0.15 \pm 0.08$ (13 mbar)	414	Salter et al., 2013b	(l)
= $0.40 \pm 0.18$ (12.6 mbar)	409		
= $0.45 \pm 0.09$ (12.6 mbar)	404		
= $1.27 \pm 0.06$ (12.6 mbar)	400		
= $1.78 \pm 0.04$ (13.0 mbar)	395		
= $1.40 \pm 0.10$ (46.7 mbar)	390		
= $1.36 \pm 0.03$ (47.5 mbar)	386		
= $1.66 \pm 0.02$ (46.7 mbar)	382		
= $1.40 \pm 0.06$ (278 mbar)	355		
$\phi^0 = 2.0$ (233 – 323 K)	>390		
$\phi^0 = 2.02 \pm 0.02$ (298 K)	382		
$\phi^0 = 1.60 \pm 0.06$ (298 K)	355		

---

### Comments

- (a) Conventional spectrophotometric study (Cary 17-D) using glyoxal pressures of ~4 mbar to 17 mbar.
- (b) Diode array spectrometer with a spectral resolution of 0.6 nm. Glyoxal, prepared by heating glyoxal trimer dihydrate in the presence of  $\text{P}_2\text{O}_5$ , was used at pressures in the range (1.5 – 10)  $\times 10^{16}$  molecule  $\text{cm}^{-3}$ .
- (c) Diode array spectrometer with a spectral resolution of 0.25 nm. Glyoxal, prepared as in (b), was used at a range of pressures but small deviations from Beer-Lambert law were found at partial pressures  $> \sim 0.4$  mbar. Cross sections reported were determined in the linear region with bath gas up to 960 mbar.
- (d) High-resolution absorption cross-sections of glyoxal were recorded at 296 K in the ultraviolet and visible (UV-vis: 19000-40000  $\text{cm}^{-1}$ , 250-526nm) and infrared (IR: 1200-8000 $\text{cm}^{-1}$ ) spectral ranges using FTS. The UV-Vis spectra of purified  $(\text{HCO})_2$  were measured at concentrations of  $\sim(1$  to 10) mbar in 1000 mbar of  $\text{N}_2$  bath gas, in a long-path (1.64 m) cell, with a spectral resolution of 0.001 nm.
- (e) Rate of photolysis of glyoxal in air mixtures at atmospheric pressure measured in an environmental chamber. The quantum yield for the photodissociation of glyoxal was obtained by comparison of the measured rate of removal of glyoxal with the rate of photolysis of  $\text{NO}_2$  under similar experimental conditions.

- (f) Laser photolysis of 5.3 mbar glyoxal in 1.3 bar N<sub>2</sub> at 295 K. HCO product determined by time-resolved laser resonance absorption. Quantum yield determined by comparing the HCO radical absorption observed with the same signals following HCHO and (CHO)<sub>2</sub> photolyses.
- (g) Excimer laser photolysis of flowing glyoxal-N<sub>2</sub> mixtures. [HCO] monitored by time-resolved cavity ring-down spectroscopy. Yields of HCO determined by comparison of absorption with signals from photolysis of formaldehyde-N<sub>2</sub> mixtures under similar conditions. Incident light intensities were measured by a Joulemeter calibrated by chemical actinometry. The HCO quantum yields were found to be independent of glyoxal pressure, total pressure (26 mbar to 470 mbar), and light intensity.
- (h) Pulsed dye laser photolysis of glyoxal-N<sub>2</sub> mixtures at 10 nm intervals in the 290-420 nm region coupled with cavity ring-down spectroscopy to monitor HCO. Absorption cross sections of glyoxal were measured. The HCO quantum yield was dependent on photodissociation wavelength, on glyoxal pressure (at all  $\lambda$ ), and nitrogen buffer gas pressure (only at  $\lambda > 320$  nm). Zero pressure HCO radical yields,  $\phi^0(\text{HCO})$ , and the ratios of quenching to unimolecular decay rate constants of excited glyoxal ( $\lambda > 320$  nm) obtained from Stern-Volmer plots are reported. The  $\phi^0(\text{HCO})$  values increase with wavelength from 290 nm to a peak of 2.0 at 390 nm, consistent with a predominance of channel (2); yields fall off rapidly above the maximum.
- (i) The photolysis of glyoxal in synthetic air was investigated in a quartz cell at 298 K using UV light sources covering the separate ranges: 275–380 nm; 390–470 nm; and 254 nm. Reactant and stable products (CO, HCHO and HCOOH) concentrations were quantitatively analyzed using long-path FTIR spectroscopy. Absolute quantum yields for overall photolysis of glyoxal and products were determined using Cl<sub>2</sub> and Br<sub>2</sub> as actinometers. Photolysis in the 390–470 nm range corresponds to the first absorption band of glyoxal, occurred with an overall quantum yield  $\phi = 0.97 \pm 0.05$ , independent of total pressure from 100 to 700 Torr air. In the range 275–380 nm, corresponding mostly to the second absorption band of glyoxal,  $\phi$  showed a dependency on total pressure, which can be expressed as a Stern–Volmer-type equation  $1/\phi = 6.80 + 251.8 \times 10^{-4} \times P$  (Torr). Analysis of product quantum yields and data from previous studies of Chen and Zhu (2003) and Calvert and Lane (1953) allowed calculation of wavelength-resolved quantum yields over the range 225–445 nm for each of the channels (1), (2) and (3). The mean photolysis rate of glyoxal under solar radiation was measured in an outdoor chamber; the rate corresponded to  $\phi = 0.035 \pm 0.007$ .
- (j) Quantum yields were measured at 85 wavelengths over the range 290-420 nm using PLP-CRDS, at pressures between 50 and 550 Torr (N<sub>2</sub>) at 298 K. HCO photolysis quantum yields from glyoxal were determined relative to HCO produced following the photolysis of mixtures of Cl<sub>2</sub> and H<sub>2</sub>CO and Cl<sub>2</sub>. Stern-Volmer analysis used to obtain extrapolated zero-pressure HCO quantum yields,  $\phi^0_{\text{HCO}}(\lambda)$ , and values for the ratio of the rate coefficients for quenching and dissociation,  $k_q/k_d(\lambda)$ , at each wavelength.  $\phi^0(\lambda)$  varied smoothly with wavelength in the range 290-420 nm, with three distinct wavelength regions: a central broad maximum region with  $\phi^0_{\text{HCO}} \sim 1.8$  between 340 and 385 nm, with  $\phi^0_{\text{HCO}}$  values decreasing at higher  $\lambda$  to near 0 at 420 nm, and at lower  $\lambda$ ,  $\phi^0$  decreasing to 0.4 at the lowest wavelength studied, 290 nm. The boundaries of these regions correlate with the photolysis thresholds for channels (2) and (4). The values of  $k_q/k_d(\lambda)$  in the range 290-420 nm were described well by an exponential function:

$$\frac{k_q}{k_d}(\lambda) = (2.3 \times 10^{-20}) + (1.5 \times 10^{-19}) \exp(-0.0957\Delta E)$$

where  $\Delta E = ((119400/\lambda - 303.0) \text{ (kJ mol}^{-1}\text{)})$  and  $\lambda$  the excitation wavelength in nm. Revised wavelength-dependent photolysis rates for the atmospheric photolysis of glyoxal, with branching ratios were presented for the production of 2HCO, H<sub>2</sub>CO + O<sub>2</sub>, and H<sub>2</sub> + 2CO at atmospheric pressure, based on analysis of these results together with the product yields reported by Tadjic et al (2006).

- (k) The formation of HCO and of H in the photolysis of glyoxal were investigated over the ranges  $\lambda = 310\text{--}335$  nm for HCO and  $\lambda = 193\text{--}340$  nm for H. Dye laser photolysis was coupled with CRDS for HCO, and with LIF for H. Absolute quantum yields were determined using

actinometers based on (a) Cl<sub>2</sub> photolysis and the Cl + HCHO reaction for HCO and (b) N<sub>2</sub>O photolysis (and O<sup>1</sup>D + H<sub>2</sub>) and CH<sub>2</sub>CO photolysis (and CH<sub>2</sub> + O<sub>2</sub>) for H. The quantum yields were found to be pressure independent, and were used to calculate yields for all product channels under atmospheric conditions.

- (l) The photolysis of glyoxal was investigated in the  $\lambda = 355\text{--}414$  nm region by dye laser photolysis coupled with CRDS. Absolute  $\phi(\text{HCO})$  was determined using the reaction of chlorine atoms with HCHO as an actinometer. The dependence of  $\phi(\text{HCO})$  on pressure was investigated at 3 to 400 Torr of N<sub>2</sub> and at four temperatures: 233 K, 268 K, 298 K and 323 K. For  $355 \text{ nm} \leq \lambda < 395 \text{ nm}$  the HCO quantum yield is pressure dependent, with linear Stern–Volmer plots ( $1/\phi(\text{HCO})$  vs. pressure). The zero pressure quantum yield,  $\phi^0_{\text{HCO}}$  obtained by extrapolation of these plots, rises from 1.6 to 2 between 355 and 382 nm and remains at 2 up to 395 nm. For  $\lambda \geq 395 \text{ nm}$   $\phi(\text{HCO})$  shows a stronger pressure dependence and non-linear SV plots, compatible with formation of HCO by dissociation from two electronic states of glyoxal with significantly different lifetimes. These observations are used to develop a mechanism for the photolysis of glyoxal over the wavelength range studied.

### Preferred Values

#### Absorption cross-sections<sup>a</sup> ( $10^{-20} \text{ cm}^2 / \text{molecule}$ ) at 296 K

$\lambda$ (nm)	$\sigma/\text{cm}^2$						
250	1.725	306	3.223	362	0.706	418	7.873
251	1.520	307	3.200	363	0.639	419	9.134
252	1.477	308	3.146	364	0.680	420	5.602
253	1.545	309	3.123	365	0.665	421	7.188
254	1.596	310	3.100	366	0.743	422	6.990
255	1.667	311	3.222	367	0.860	423	13.045
256	1.619	312	3.343	368	1.012	424	8.239
257	1.809	313	3.390	369	1.063	425	10.448
258	1.823	314	3.233	370	1.139	426	16.411
259	1.850	315	2.805	371	1.185	427	16.101
260	1.828	316	2.646	372	1.141	428	21.424
261	1.957	317	2.460	373	1.212	429	6.499
262	2.027	318	2.214	374	1.352	430	7.027
263	2.144	319	1.927	375	1.332	431	6.518
264	2.184	320	1.854	376	1.377	432	6.082
265	2.261	321	1.885	377	1.467	433	5.657
266	2.333	322	1.766	378	1.605	434	6.809
267	2.371	323	1.723	379	1.534	435	7.660
268	2.361	324	1.677	380	1.934	436	13.187
269	2.475	325	1.603	381	2.455	437	9.185
270	2.509	326	1.606	382	2.019	438	13.822
271	2.613	327	1.695	383	2.069	439	12.135
272	2.720	328	1.937	384	1.939	440	25.942
273	2.810	329	1.857	385	1.893	441	13.118
274	2.920	330	1.689	386	1.835	442	9.013
275	3.000	331	1.128	387	2.287	443	11.124
276	3.060	332	1.048	388	3.000	444	13.460
277	3.087	333	0.966	389	3.206	445	15.110
278	3.078	334	0.919	390	3.483	446	7.818
279	3.086	335	0.737	391	3.922	447	3.730
280	3.135	336	0.630	392	3.801	448	4.144
281	3.216	337	0.589	393	2.852	449	5.527
282	3.322	338	0.647	394	3.147	450	8.682
283	3.455	339	0.585	395	3.855	451	13.817
284	3.568	340	0.553	396	3.679	452	15.945
285	3.673	341	0.563	397	3.361	453	30.368

286	3.797	342	0.510	398	4.323	454	26.902
287	3.791	343	0.499	399	4.345	455	51.990
288	3.813	344	0.649	400	3.873	456	15.666
289	3.800	345	0.624	401	4.455	457	2.661
290	3.734	346	0.733	402	5.843	458	2.201
291	3.643	347	0.631	403	7.159	459	0.902
292	3.654	348	0.604	404	6.237	460	1.202
293	3.681	349	0.415	405	4.491	461	0.883
294	3.729	350	0.391	406	4.482	462	0.588
295	3.809	351	0.395	407	4.066	463	0.322
296	3.824	352	0.423	408	3.444	464	0.339
297	3.922	353	0.415	409	4.008	465	0.330
298	4.073	354	0.403	410	5.661	466	0.416
299	4.123	355	0.422	411	7.221	467	0.522
300	4.045	356	0.443	412	7.406	468	0.149
301	3.905	357	0.431	413	10.753	469	0.091
302	3.779	358	0.471	414	10.115	470	0.076
303	3.567	359	0.503	415	10.194	471	0.086
304	3.350	360	0.546	416	6.073	472	0.092
305	3.242	361	0.627	417	6.829	473	0.110

a: Averaged over 1 nm intervals, and given for the central wavelength of each interval.

### Zero Pressure quantum yields for HCO radical and H atom at 298 K

$$\phi_{\text{HCO}}^0(\lambda) = 2.013 + (0.465 - 2.013)/(1 + \exp((\lambda - 333.4)/15.55))$$

$$\phi_{\text{H}}^0(\lambda) = 0.0209 + (0.924 - 0.0209)/(1 + \exp((\lambda - 296)/26.21))$$

### Zero Pressure quantum yields for HCO at 298 K

$\lambda(\text{nm})$	$\phi^0(\text{HCO})$	$\lambda(\text{nm})$	$\phi^0(\text{HCO})$	$\lambda(\text{nm})$	$\phi^0(\text{HCO})$
290	0.554	335	1.279	380	1.94
295	0.586	340	1.401	385	1.96
300	0.627	345	1.515	390	1.97
305	0.680	350	1.617	395	1.98
310	0.746	355	1.704	400	1.99
315	0.828	360	1.776	405	2.00
320	0.925	365	1.834	410	2.00
325	1.035	370	1.879	415	2.00
330	1.155	375	1.913	420	2.00

### Zero Pressure quantum yields for channels (2) – (5) at 298 K

$$\phi_2^0(\lambda) = 2/(1 + \exp((\lambda - 330.0)/14.1))$$

$$\phi_3^0(\lambda) = (1 - (\phi_2(\lambda) + \phi_4(\lambda) + \phi_5(\lambda)))$$

$$\phi_4^0(\lambda) = 0.0 + (0.39 - 0.0)/(1 + \exp((\lambda - 331.7)/-14.0))$$

$$\phi_5^0(\lambda) = 0.56 + (0.0 - 0.56)/(1 + \exp((\lambda - 276.7)/12.0))$$

### Pressure dependence of glyoxal photolysis quantum yields

$$\varphi_{total}(\lambda, M, T) = 1 / \left( \frac{1}{\varphi_2^0 + \varphi_3^0 + \varphi_4^0 + \varphi_5^0} \right) \times \left( \frac{(1 + A_1[M] + A_2)(1 + A_3[M])}{(1 + A_2 + A_3[M])} \right)$$

where [M] is molecule cm<sup>-3</sup> and  $A_1$ ,  $A_1$  and  $A_1$ , are parameters given as a function of temperature  $T$  and wavelength  $\lambda$  by the following expressions:

$$A_1 = [a_{11} \times (T/295)^{a_{12}}] \times \left( \exp[a_{13} \times (T/295)^{a_{14}}] \times \left\{ \frac{10^7}{\lambda} - 23800 \right\} \right)$$

$$A_2 = [a_{21} \times (T/295)^{a_{22}}] \times \left( \exp[a_{23} \times (T/295)^{a_{24}}] \times \left\{ \frac{10^7}{\lambda} - 23800 \right\} \right)$$

$$A_3 = [a_{31} \times (T/295)^{a_{32}}] \times \left( \exp[a_{33} \times (T/295)^{a_{34}}] \times \left\{ \frac{10^7}{\lambda} - 23800 \right\} \right)$$

The table below gives the constants listed in the above equations to calculate the quantum yield for glyoxal photolysis as a function of temperature and pressure,; x = 1,2 or 3 in above equations for A1, A2, and A3 respectively. Errors are 1 $\sigma$ .

#### Parameters for calculation of pressure dependence of quantum yields

parameter	$a_{x,1}$	$a_{x,2}$	$a_{x,3}$	$a_{x,4}$
$A_1$	$(6.48 \pm 0.48) \times 10^{-19}$	$-1.83 \pm 0.48$	$0.000760 \pm 0.00005$	$-0.515 \pm 0.360$
$A_2$	$112.8 \pm$	$-1.53 \pm 0.31$	$0.00461 \pm 0.00006$	$0.507 \pm 0.117$
$A_3$	$(2.25 \pm 0.31) \times 10^{-16}$	$-9.18 \pm 0.78$	$0.000780 \pm 0.00032$	$-7.03 \pm 1.58$

#### Quantum yields at 1 bar and 298 K

$\lambda$ (nm)	$\phi(2)$	$\phi(3)$	$\phi(4)$	$\phi(5)$	$\phi(\text{total})$	$\phi^0(\text{HCO})$
	2HCO	HCHO+CO	HCO+CO+H	2H+2CO	1bar, 298K	1bar, 298K
190	0.000	0.050	0.390	0.560	1.000	0.390
195	0.000	0.051	0.390	0.559	1.000	0.390
200	0.000	0.051	0.390	0.559	1.000	0.390
205	0.000	0.051	0.390	0.559	1.000	0.390
210	0.000	0.052	0.390	0.558	1.000	0.390
215	0.001	0.053	0.390	0.557	1.000	0.390
220	0.001	0.055	0.390	0.555	1.000	0.391
225	0.001	0.057	0.390	0.553	1.000	0.391
230	0.001	0.061	0.390	0.549	1.000	0.391
235	0.001	0.066	0.390	0.543	1.000	0.392
240	0.002	0.074	0.389	0.535	1.000	0.393
245	0.002	0.086	0.389	0.523	1.000	0.394
250	0.004	0.102	0.389	0.505	1.000	0.396
255	0.005	0.126	0.388	0.481	1.000	0.398
260	0.007	0.157	0.388	0.448	1.000	0.401
265	0.010	0.197	0.387	0.407	1.000	0.406
270	0.014	0.245	0.385	0.356	0.999	0.413
275	0.020	0.297	0.383	0.300	0.999	0.422
280	0.028	0.350	0.381	0.242	0.998	0.436
285	0.040	0.397	0.377	0.187	0.997	0.454
290	0.056	0.435	0.371	0.139	0.995	0.480
295	0.077	0.459	0.364	0.100	0.992	0.514
300	0.106	0.470	0.353	0.070	0.989	0.560
305	0.145	0.467	0.340	0.048	0.983	0.619

310	0.195	0.451	0.322	0.033	0.975	0.693
315	0.257	0.422	0.299	0.022	0.963	0.782
320	0.330	0.383	0.272	0.015	0.947	0.882
325	0.412	0.337	0.241	0.010	0.925	0.986
330	0.500	0.287	0.207	0.007	0.897	1.083
335	0.587	0.236	0.172	0.004	0.861	1.160
340	0.670	0.188	0.139	0.003	0.816	1.208
345	0.743	0.146	0.109	0.002	0.763	1.218
350	0.805	0.111	0.083	0.001	0.702	1.189
355	0.855	0.082	0.062	0.001	0.635	1.125
360	0.893	0.060	0.046	0.001	0.564	1.033
365	0.923	0.044	0.033	0.000	0.492	0.925
370	0.945	0.031	0.024	0.000	0.423	0.809
375	0.961	0.022	0.017	0.000	0.358	0.694
380	0.972	0.016	0.012	0.000	0.300	0.586
385	0.980	0.011	0.008	0.000	0.248	0.489
390	0.986	0.008	0.006	0.000	0.204	0.403
395	0.990	0.006	0.004	0.000	0.165	0.327
400	0.993	0.004	0.003	0.000	0.129	0.257
405	0.995	0.003	0.002	0.000	0.093	0.185
410	0.997	0.002	0.001	0.000	0.055	0.109
415	0.998	0.001	0.001	0.000	0.024	0.048
420	0.000	0.001	0.001	0.000	0.008	0.016

### Comments on Preferred Values

Glyoxal exhibits two distinct absorption regions relevant for atmospheric photolysis. The first region consists of a series of discrete bands between 360 – 460 nm, super-imposed on a continuum. The second region shows a broad band with some structure and a maximum absorption near 300 nm. The preferred values for the absorption cross-sections are based on the high resolution data determined by Volkamer *et al.* (2006) and are averaged over 1 nm intervals around the central wavelength. These data are on average 5–8% larger than the values measured by Horowitz *et al.* (2001), which are in excellent agreement with the data of Orlando and Tyndall (2001) at  $\lambda > 240$  nm, and in satisfactory agreement with the earlier data of Plum *et al.* (1983). The cross sections from Horowitz *et al.* (2001) and Volkamer *et al.* (2006) averaged over 2 nm are plotted in Fig. 1. Data at other resolution can be found in and in the MPG website (<http://www.atmosphere.mpg.de/enid/>).

Plum *et al.* (1983) showed that the overall quantum efficiency in the first absorption region (325–470 nm) is only ~3%, and this is confirmed in the detailed product analysis study of glyoxal photolysis by Tadjic *et al.* (2005), which also indicated the occurrence of both radical and molecular dissociation pathways, and a fall off in overall  $\phi$  at  $\lambda > 350$  nm. The results of Langford and Moore (1984), Zhu *et al.* (1996), Chen and Zhu (2003), Feierabend, *et al.* (2009) and Salter *et al.* (2013a, 2013b), in which the wavelength-resolved quantum yields of the HCO photolysis product was determined directly, shows that dissociation to HCO radicals is a major pathway at all wavelengths less than the dissociation threshold for channel (2) (412 nm), and is even observed up to 420 nm. It is the predominant product in the region of importance for atmospheric photolysis. The studies also show that  $\phi(\text{HCO})$  is subject to pressure quenching by  $\text{N}_2$  following a Stern-Volmer model. Salter *et al.* (2013a) have also determined the wavelength-resolved, zero pressure quantum yields of the H-atoms from glyoxal photolysis in the range  $\lambda = 193 - 340$  nm, which confirmed that channel 4 occurred up to its threshold near  $\lambda = 342$  nm. This accounts for the CO formation attributed in previous work to channel (1) (Tadjic *et al.* (2005), Feierabend, *et al.* (2009)). The results of Salter *et al.* (2013a) for HCO and H formation at 193 nm show that channel (5):  $(\text{HCO})_2 + h\nu \rightarrow 2\text{H} + \text{CO}$  ( $\lambda_{\text{threshold}} = 291$  nm) is also operative, presumably *via* dissociation of HCO formed in channel 4. Analysis of the body of data by Salter *et al.* (2013b) showed that for the wavelength region of interest for atmospheric chemistry (290 - 414 nm) only three radical channels (2, 4 and 5) and one molecular channel (3) were involved in glyoxal photolysis.

These channels can all be rationalised in terms of the generally accepted mechanism proposed by Chen and Zhu (2003), involving excitation to a vibrationally excited  $S^*_1$  state which then undergoes decomposition, collisional quenching, or intersystem crossing to an excited triplet state,  $T^*_1$ . This state also undergoes decomposition or collisional quenching. The major product HCO can derive from either state. In general there is a consistent picture for glyoxal photolysis, but there are some discrepancies in the reported data. The  $\phi^0(\text{HCO})$  values of Feierabend et al. (2009) are up to a factor of two lower than those of Chen and Zhu (2003), and the wavelength dependence of HCO quantum yield derived by Tadic et al (2006) differs significantly from both direct studies, suggesting difficulties in interpretation of HCO yields from the end-product measurements. Feierabend et al (2009) have shown that secondary gas phase production of HCO accounts for part of the HCO yield observed at  $\lambda > 400$  nm under some conditions. A mechanism is proposed which involves an energy pooling reaction between two glyoxal molecules in the triplet  $T_1$  state, which has been confirmed in an independent PLP-CRDS study by Salter et al. (2009). This complication likely affected the measurements of Chen and Zhu (2003), who used relatively high glyoxal concentrations, but was not important under the conditions employed in the measurements of  $\phi(\text{HCO})$  at  $\lambda > 400$  nm by Feierabend et al (2009), or those of Salter et al. (2013a, 2013b).

There are also conflicting results for quenching parameters,  $k_q/k_d$  and zero pressure quantum yields,  $\phi^0(\text{HCO})$ , which are determined from Stern-Volmer plots of the pressure dependence of the quantum yields. At  $\lambda < 380$  nm Salter et al. (2013a) observed no pressure quenching for HCO yields in the range  $\lambda = 310\text{--}335$  nm which differs significantly from the results of Feierabend et al (2009) who found that quenching of  $\phi(\text{HCO})$  persisted down to 290 nm. Tadic et al. (2006) observed no pressure quenching for glyoxal photolysis in the range  $275 < \lambda < 380$ , which supports the conclusion of Salter et al. (2013a). There is no obvious explanation of this discrepancy.

The zero pressure quantum yield,  $\phi^0(\text{HCO})$  from channel (2) increases with  $\lambda$  above 355 nm and is close to 2 for  $\lambda > 380$  nm. At longer wavelengths ( $\lambda > 395$  nm),  $\phi(\text{HCO})$  determined by Salter et al (2013b) gave non-linear Stern-Volmer plots, which they attribute to formation of HCO from two states, whose lifetime differs by up to 2 orders of magnitude. Although this non-linearity was not observed by Chen and Lui (2003) or by Feierabend et al. (2009) in the higher range of pressure they used, and their  $\phi^0(\text{HCO})$  values at  $\lambda > 400$  nm obtained by linear extrapolation of their Stern-Volmer plots were increasingly lower than those reported by Salter et al who used a 2-state quenching model. There is considerable experimental uncertainty in the accurate determination of  $\phi^0(\text{HCO})$  from the intercepts in the non-linear region, but Salter et al. postulate a unit zero pressure quantum yield (i.e.  $\phi^0(\text{HCO}) = 2$ ) extending above 400 nm on the basis of their extended low pressure data, as opposed to a decline in  $\phi^0(\text{HCO})$  values  $\lambda > 395$  nm suggested by Feierabend et al. (2009).

The experimental zero pressure yields for  $\phi^0_{\text{HCO}}(\lambda)$  were fitted as a function of wavelength to a Boltzmann function of the form:

$$\phi^0_{\text{HCO}}(\lambda) = B_2 + (B_1 - B_2) / (1 + \exp((\lambda - x_0)/dx))$$

where wavelength is in nm, to obtain the preferred values of  $\phi^0_{\text{HCO}}(\lambda)$ . The parameters for the zero pressure quantum yields of HCO were obtained from simultaneously fitting the zero pressure yields of  $\phi_{0,\text{HCO}}(\lambda)$  of Salter et al. (2013a,b) and Chen and Zhu (2003), with the constraint of a value of  $\phi^0_{\text{HCO}} = 2$ , at  $\lambda > 400$  nm. The data of Feireabend et al (2008) were not used in this fitting in view of the inconsistencies referred to above. The yield of H was obtained from a fit to  $\phi_{0,\text{H}}(\lambda)$  values from (Salter et al., 2013a) which showed no pressure dependence, with a constraint that  $\phi_4$  and  $\phi_5 = 0$  for wavelengths  $> 342$  nm and  $> 291$  nm respectively. The zero pressure yields for the individual product channels (2), (4) and (5) were also represented by the above equation with the parameters obtained from fitting the values of  $\phi^0_{\text{HCO}}(\lambda)$  and  $\phi^0_{\text{H}}(\lambda)$  of Salter et al., 2013a,b, the  $\phi_{0,\text{HCO}}(\lambda)$  of Chen and Zhu,

(2003) and  $\phi_{0,\text{HCHO}}(\lambda)$  (254 nm) from Tadic et al. (2006).  $\phi_3(\lambda)$  (channel 3) is obtained from  $1 - (\phi_2(\lambda) + \phi_4(\lambda) + \phi_5(\lambda))$ . The values of  $\phi_2^0$ ,  $\phi_3^0$ ,  $\phi_4^0$ , and  $\phi_5^0$  at 298 K are plotted as a function of  $\lambda$  in Figure 2.

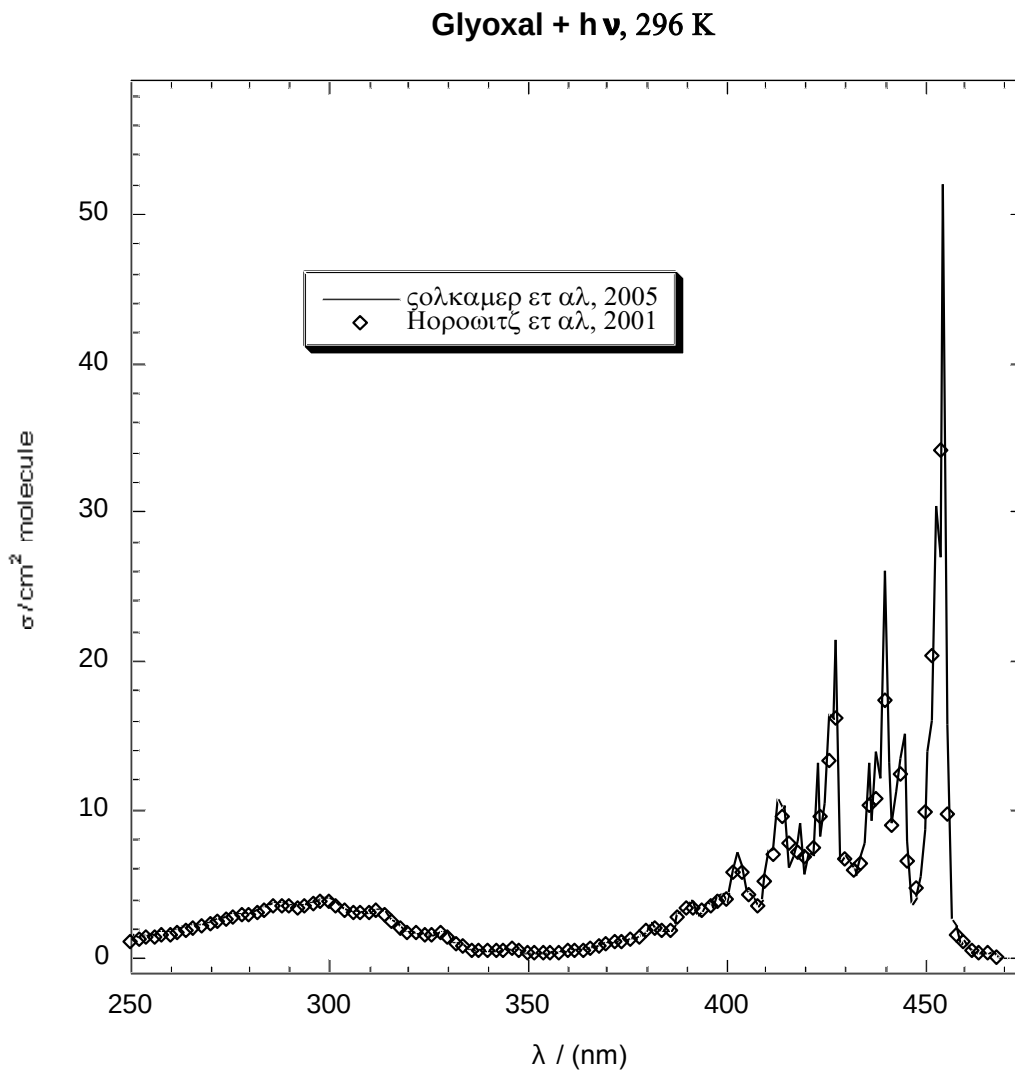
The preferred values of  $\phi_{\text{total}}$  for glyoxal photolysis at any wavelength, temperature and pressure are given by the extended Stern-Volmer equation proposed by Salter et al. (2013) using the 2-state quenching model. The parameters needed to calculate  $A_1$ ,  $A_2$  and  $A_3$  are given in the table in the preferred values section above, which were derived by Salter et al., from a standard linear least squares fit to all the HCO data (except those of Feireabend et al (2008)), weighted to account for the experimental errors. These apply to pressure dependence of individual channels and to the total glyoxal photolysis by all channels. The recommended  $\phi$  values applying at 1 bar pressure and 298 K, for all channels in atmospheric photolysis and for the overall photolysis, are also shown in a table. The values of  $\phi_{\text{total}}$  at 1 bar are plotted together with  $\phi(\text{HCO})$  in figure 3.

Generally the parameterisation reproduces the experimental observations quite well. Uncertainties in atmospheric photolysis rates mostly arise from the assumptions made in selecting and fitting the experimental data. Because there is significant atmospheric photolysis between 300 - 360 nm, the significant differences in the observations in this region are a cause for concern; as a measure of uncertainty the glyoxal photolysis rate calculated using the quantum yields recommended by Feireabend et al.(2008) is 20% lower than calculated from the preferred values adopted here. On the other hand uncertainty arising from the different adopted Stern-Volmer quenching model between 395 - 415 nm does not contribute very significantly to the overall photolysis of glyoxal in the lower atmosphere.

## References

- Calvert, J.G. and Lane, G.S., J.Amer.Chem.Soc., 75 856, 1953.
- Chen, Y.Q. and Zhu, L., J. Phys. Chem.A, 107, 4643, 2003.
- Feierabend, K. J.; Flad, J. E.; Brown, S. S.; Burkholder, J. B., J. Phys. Chem. A, 113, 7784 -7794, 2009.
- Horowitz, A., Meller, R. and Moortgat, G. K., J Photochem.Photobiol., A: Chem. 146, 19, 2001.
- Klotz, B., Graedler, F., Sorenson, S., Barnes, I. and Becker, K.-H., Int. J. Chem. Kinet. 33, 9, 2000.
- Langford, A. O. and Moore, C. B., J. Chem. Phys. 80, 4211, 1984.
- Li, X. and Schlegel, H. B., J. Chem. Phys. 114, 8, 2001.
- Orlando, J. J. and Tyndall, G. S., Int. J. Chem. Kinet., 33, 149, 2001.
- Plum, C. N., Sanhueza, E., Atkinson, R., Carter, W. P. L. and Pitts, Jr., J. N., Environ. Sci. Technol. 17, 479, 1983.
- Salter, R.J., Blitz, M.A., Heard, D.E. Pilling, M.J., and Seakins, P.W., J.Phys.Chem. A, 113, 8278-8285, 2009.
- Salter, R. J., Blitz, M. A., Heard, D. E., Kovacs, T., Pilling, M. J., Rickard, A. R. and Seakins, P. W., Phys. Chem. Chem. Phys., 15, 4984, 2013.
- Salter, R. J., Blitz, M. A., Heard, D. E., Pilling, M. J., Rickard, A. R. and Seakins, P. W., Phys. Chem. Chem. Phys., 15, 6516, 2013.
- Tadjic, J., Moortgat, G.K., and Wirtz, K., Journal of Photochemistry and Photobiology A: Chemistry 177 (2006) 116-124.
- Volkamer, R., J Photochem. Photobiol. A: Chemistry, 172, 35-46, 2005.
- Zhu, L., Kellis, D. and Ding, C.-F., Chem. Phys. Lett. 257, 487, 1996.

**Figure 1:** Comparison of absorption cross sections from Volkamer et al, 2006 (averaged over 2 nm) and from Horowitz et al, 2001 (averaged over 2 nm as presented in the compilation at <http://www.atmosphere.mpg.de/enid/>)



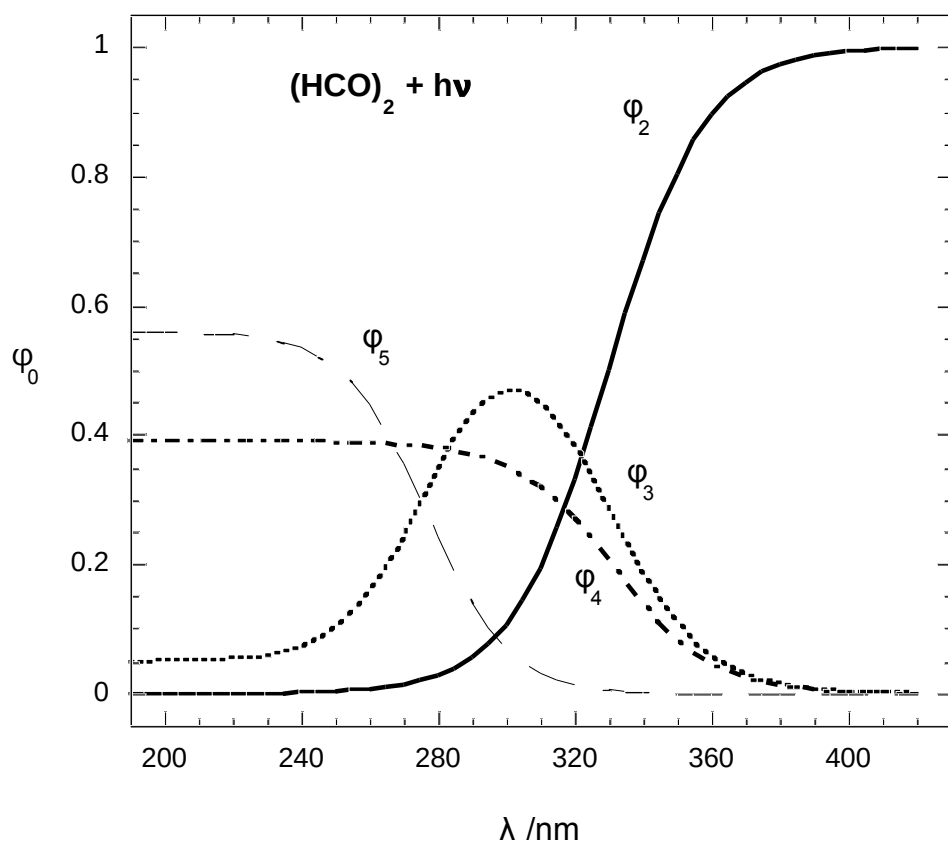


**Figure 2:** Preferred values for wavelength dependence of zero pressure quantum yields for channels (2), (3), (4) and (5) in glyoxal photolysis at 298 K

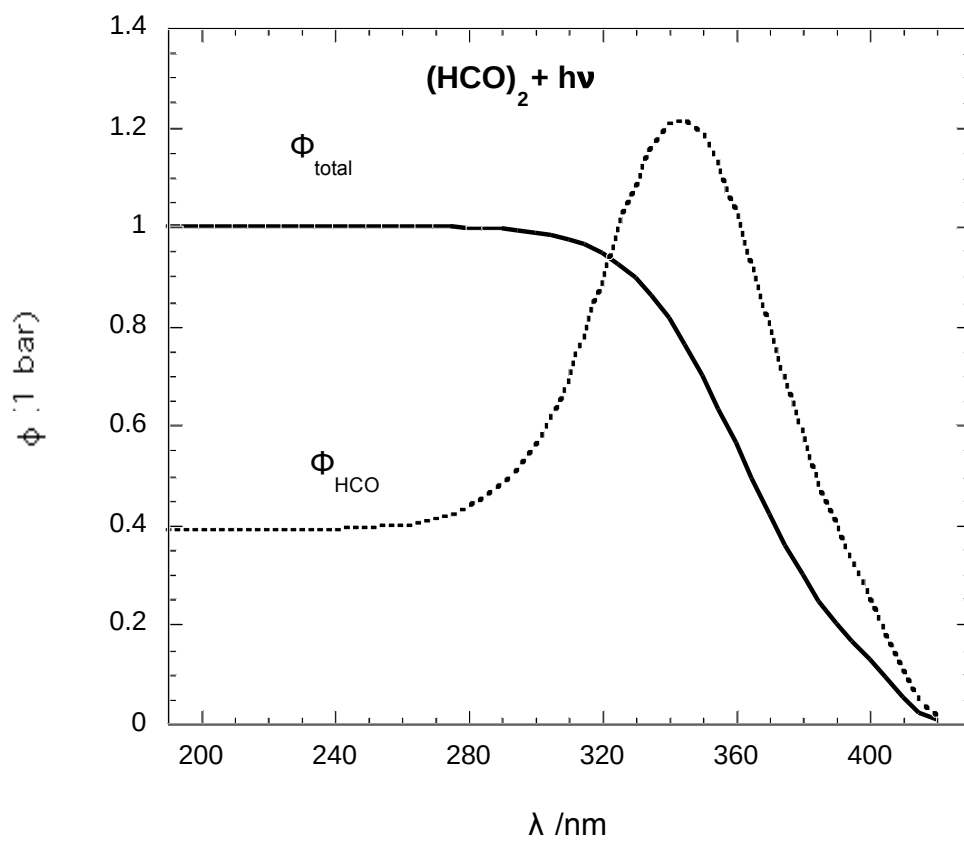


**Figure 3:** Wavelength dependence of quantum yield for overall glyoxal photolysis and HCO production, at 1 bar pressure and 298 K.